© 2014. Published by The Company of Biologists Ltd | Journal of Cell Science (2014) 127, 1043–1051 doi:10.1242/jcs.140921

RESEARCH ARTICLE

The Mon1–Ccz1 GEF activates the Rab7 GTPase Ypt7 via a longin-fold–Rab interface and association with PI3P-positive membranes

Margarita Cabrera[1], Mirjana Nordmann[1,*], Angela Perz[1], David Schmedt[2], Andreas Gerondopoulos[3], Francis Barr[3], Jacob Piehler[2], Siegfried Engelbrecht-Vandré[1] and Christian Ungermann[1,‡]

ABSTRACT

To function in fusion and signaling, Rab GTPases need to be converted into their active GTP form. We previously identified the conserved Mon1–Ccz1 complex as the guanine nucleotide exchange factor (GEF) of the yeast Rab7 GTPase Ypt7. To address the possible GEF mechanism, we generated a homology model of the predicted longin domains of Mon1 and Ccz1 using the Rab-binding surface of the TRAPP complex as a template. On the basis of this, we identified mutations in both yeast Mon1 and Ccz1 that block Ypt7 activation, without affecting heterodimer formation and intracellular localization of Mon1 and Ccz1 at endosomes. Strikingly, the activity of the isolated Mon1–Ccz1 complex for Ypt7 is highly stimulated on membranes, and is promoted by the same anionic phospholipids such as phosphatidylinositol-3-phosphate (PI3P), which also support membrane association of the GEF complex. Our data imply that the GEF activity of the Mon1–Ccz1 complex towards Rab7/Ypt7 requires the interface formed by their longin domains and profits strongly from its association with the organelle surface.

KEY WORDS: Guanine nucleotide exchange factor, Mon1–Ccz1, Rab GTPase, Endosome, Membrane fusion

INTRODUCTION

Within the endomembrane system, vesicles transport cargo between organelles. These organelles need to maintain their identity despite the fact that they continuously fuse with incoming vesicles and lose membrane as a result of vesicle generation. Rab GTPases, tethering factors and the SNARE machinery localize to specific organelles and cooperate to promote fusion of membranes. Rab proteins are small GTP/GDP-binding proteins with C-terminal prenyl anchors, which function as molecular switches. They bind in their GTP form to tethering factors to bring membranes into proximity before SNAREs present in each membrane form four-helix bundles and thus drive bilayer mixing.

[1]University of Osnabrück, Department of Biology/Chemistry, Biochemistry section, Barbarastrasse 13, 49076 Osnabrück, Germany. [2]University of Osnabrück, Department of Biology/Chemistry, Biophysics section, Barbarastrasse 13, 49076 Osnabrück, Germany. [3]Department of Biochemistry, University of Oxford, South Parks Road, Oxford OX1 3QU, UK.

*Present address: University of Osnabrück, Department of Biology/Chemistry, Section of Molecular Cell Biology, Barbarastrasse 13, 49076 Osnabrück, Germany.

‡Author for correspondence (cu@uos.de)

Received 16 August 2013; Accepted 9 December 2013

As a result of the slow rate of dissociation of GDP, Rabs require guanine nucleotide exchange factors (GEFs) for their conversion into the active GTP-bound form, which can interact with effectors on membranes such as tethering factors or lipid kinases. In addition, Rabs depend on a GTPase activating protein (GAP) to hydrolyze the GTP to GDP, and then become substrates of the GDI chaperone, which can extract the Rab-GDP and keep it soluble in the cytoplasm (Lachmann et al., 2011; Hutagalung and Novick 2011; Itzen and Goody 2011; Barr, 2013).

Among the Rab interactors, GEFs are most crucial because they provide the activated Rab at a specific location in the cell. In this context, structures of Rab–GEF complexes and the subsequent analyses have been very informative. For the exocytic Sec4 Rab, the GEF Sec2 promotes nucleotide exchange via its α-helical domain (Dong et al., 2007; Sato et al., 2007). Rab5-like proteins that operate in the endosomal pathway depend on Vps9-domain-containing GEFs (Delprato et al., 2004; Delprato and Lambright 2007). DENN domains were identified as a signature domain for multiple GEFs (Yoshimura et al., 2010; Allaire et al., 2010; Marat et al., 2011) and molecular details of their function were revealed for DENND1-BS and Rab35 (Wu et al., 2011).

GEFs might also act as part of a multiprotein complex. The best-characterized example is the heptameric TRAPPI, which interacts with the Rab1/Ypt1 protein through a surface consisting of four subunits: Bet5, Trs23 and the two flanking copies of Bet3 (Kümmel et al., 2006; Kim et al., 2006; Cai et al., 2008). GEF dimers are required to activate Rab6/Ypt6 (Ric1–Rgp1) (Pusapati et al., 2012; Siniossoglou et al., 2000) and Rab7/Ypt7 (Mon1–Ccz1) (Nordmann et al., 2010; Gerondopoulos et al., 2012), although structural information on these complexes is lacking. In agreement with the function of the Mon1–Ccz1 dimer in Ypt7 activation, endosomal biogenesis is strongly impaired if either of the two proteins is defective (Wang et al., 2002; Kinchen and Ravichandran 2010; Poteryaev et al., 2010; Nordmann et al., 2010; Yousefian et al., 2013).

TRAPP subunits Bet5 and Trs23 interact both with each other and with Ypt1 through their longin domains (Kim et al., 2006; Cai et al., 2008). These are arranged into a continuous ten-strand β-sheet supporting two parallel α-helices, which provide a significant portion of the interacting residues. Interestingly, the formation of the Mon1–Ccz1 heterodimer also requires the predicted longin domains of both subunits (Nordmann et al., 2010). This suggests that the architecture and mode of GEF action of Mon1 and Ccz1 on Ypt7 might resemble those of the TRAPPI complex. Here, we present evidence that Mon1 and Ccz1, which are linked to Rab7/Ypt7 both in mammals and yeast, cooperate

Journal of Cell Science (2014) 127, 1043–1051 doi:10.1242/jcs.140921

via their longin-domain surface to activate the Rab GTPase. This activity is strongly promoted upon membrane recruitment of the GEF, suggesting that previously determined activities might have been significantly underestimated.

RESULTS

Mon1 and Ccz1 require a common interface for Ypt7 activation

Secondary structure prediction using PredictProtein (http://predictprotein.org) and PsiPred (http://bioinf.cs.ucl.ac.uk/psipred/) identified possible longin domains in Ccz1 (aa 1–156) and Mon1 (aa 180–287), which are required for the assembly of the Mon1–Ccz1 heterodimer (Nordmann et al., 2010). This suggests a similar structure–function relationship for Mon1–Ccz1 and the TRAPPI GEF complex, because the two TRAPP subunits Trs23 and Bet5 also contain longin domains that contact the Rab GTPase Ypt1 directly (Kim et al., 2006; Cai et al., 2008). We therefore built a homology model for the predicted longin domains of Mon1–Ccz1 using Trs23 and Bet5 as templates.

Longin domains consist of a central antiparallel β-sheet (S1–S5) with one α-helix (H1) on one side and two α-helices (H2, H3) on the opposing side. Trs23 and Bet5 interact edge to edge through the central β-sheets of their longin domains and contact Ypt1 primarily through residues residing in the H1 helices of both subunits (Fig. 1A). Consequently, mutants in each H1 helix result in loss of GEF activity towards Ypt1 (Cai et al., 2008) (Fig. 1B). In addition, Ypt1 is recognized by loop S1–S2 and strand S2 of Trs23 (Fig. 1B) and some residues provided by the two copies of Bet3 (Cai et al., 2008). We used the Genesilico Metaserver (Kurowski et al., 2003) to assign Ccz1 (aa 1–156) to Bet5 and Mon1 (aa 180–287) to Trs23, and built a homology model for Ypt7/Mon1 and Ccz1 longin domains based on the Ypt1–TRAPP complex (see Materials and Methods for details). The resulting model showed only few clashes with satisfactory stereochemistry (Fig. 1C).

On the basis of this model and the previously characterized TRAPP mutants, we introduced mutations in Mon1 and Ccz1 that should interfere with GEF activity (Fig. 1D). Notably, for TRAPPI and DENND1B-S, double and triple mutants had to be generated in order to abolish GEF activity completely (Cai et al., 2008; Wu et al., 2011). We therefore used a similar approach here, and first followed vacuole morphology of Mon1 and Ccz1 mutants. Deletion of Mon1 or Ccz1 resulted in multiple small vacuoles (Fig. 2A–C). This defect was rescued by expression of Mon1 and Ccz1, either from a normal promoter or when overproduced (Fig. 2A,C). For Mon1, we identified mutations in helix H1 (G209W, T213K) and the neighboring S1–S2 region (G191P, K192D) that resulted in vacuolar defects (Fig. 2A). Defects in the single G191P mutant were only observed if expression of Mon1 was lowered (Fig. 2C). Ccz1 mutants displayed similar defects if mutated in the H1 region (G47W, G51M) (Fig. 2B). These defects were not due to mislocalization, because GFP-tagged Mon1 and Ccz1 mutants were still found in dot-like structures, which probably represent endosomes, similar to the wild-type proteins (Fig. 2D,E). To test whether any of the mutations interfered with the Rab interaction, we relied on a yeast three-hybrid assay, where both Mon1 and Ccz1 were co-expressed with Ypt7. This assay clearly demonstrated interaction of Mon1 and Ccz1 with the GDP-locked version of Ypt7 (T22N), whereas none of the mutants of Mon1 or

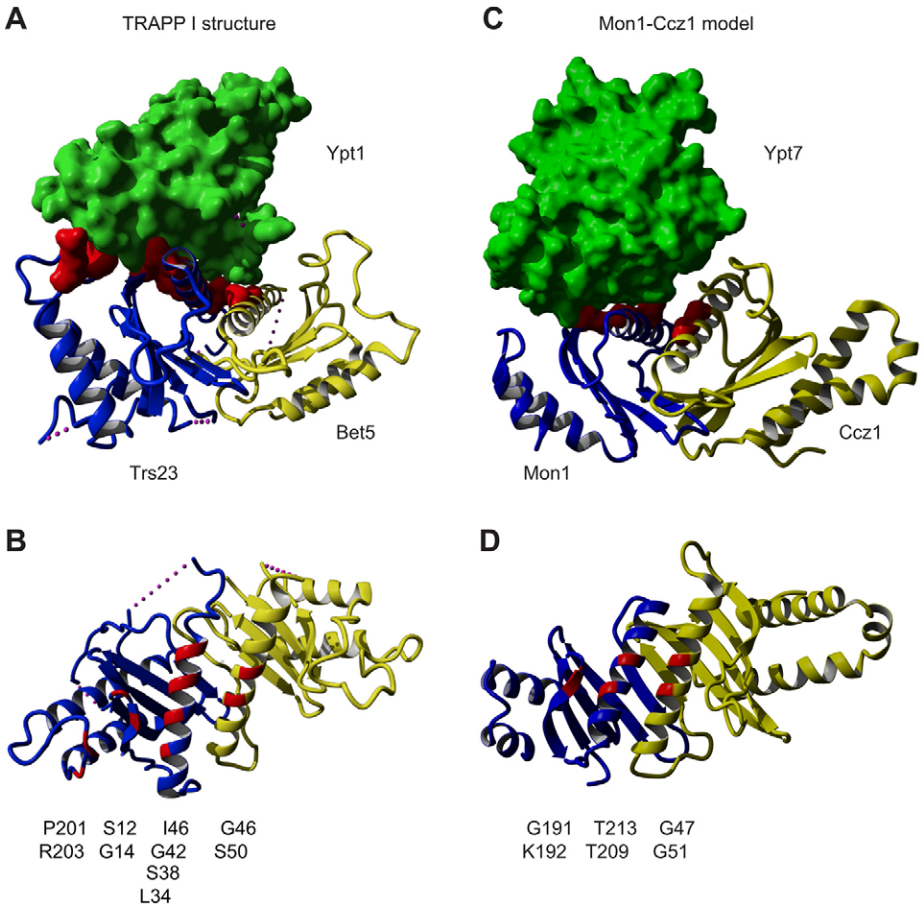

Fig. 1. Model of Mon1–Ccz1 longin domains in complex with the Rab Ypt7. (A,B) Structure of yeast TRAPP subunits Trs23 (PDB ID 3CUEa) and Bet5 (PDB ID 3CUEc). Residues forming Ypt1-binding surface are indicated in red (Cai et al., 2008). In B, The Trs23-Bet5 segment is rotated by 90° and Ypt1 is not shown. Residues of the Ypt1-binding surface are listed below the structure. (C,D) Modeling of predicted Mon1 and Ccz1 longin domains based on the structure of Trs23 and Bet5 (YASARA). Residues within Mon1 and Ccz1 longin domains, which could participate in the interaction with Ypt7-GDP (Constantinescu et al., 2002) are shown in red. Representation of the putative Rab-GEF interface is shown as in B, and postulated interacting residues are listed below the model.

Journal of Cell Science (2014) 127, 1043–1051 doi:10.1242/jcs.140921

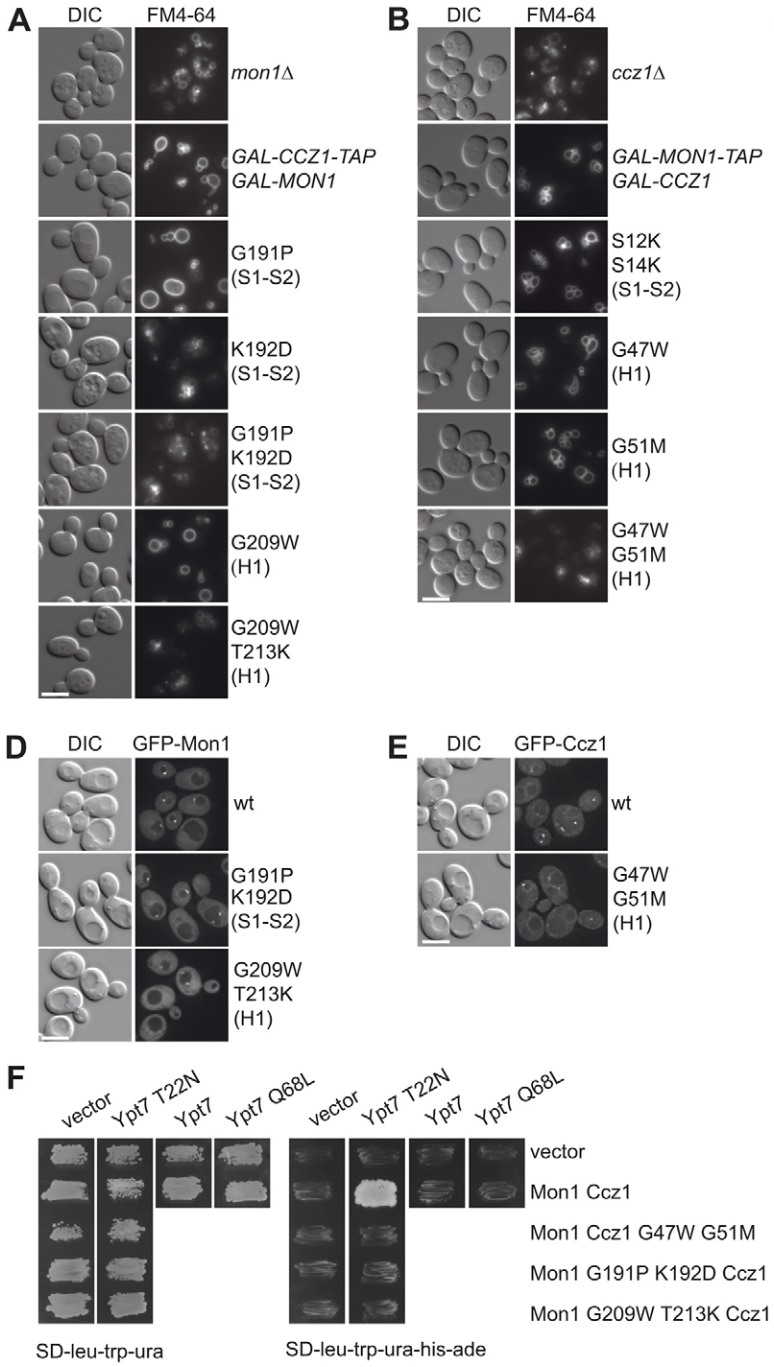

Fig. 2. Identification of mutants that affect Mon1–Ccz1 GEF activity. (A–C) Analysis of vacuole morphology in Mon1 (A,C) and Ccz1 (B) mutants. Vacuoles were stained with FM4-64 in cells overexpressing wild-type (wt) or Mon1/Ccz1 mutants. Mutations were generated based on TRAPPI GEF mutants (Cai et al., 2008) in S1–S2 and H1 regions of Mon1 and Ccz1 longin domains. In C, wild-type and mutant Mon1 was expressed from the *NOP1* promoter to reduce expression. (D,E) Localization of GFP-tagged Mon1 and Ccz1 mutants analyzed by fluorescence microscopy. Both mutants remain associated with endosomes as observed for wild-type (wt) proteins. (F) Analysis of Mon1–Ccz1 interaction with Ypt7 by yeast three-hybrid assay. Plasmids coding for Ypt7, Mon1 and Ccz1 were co-transformed in the PJ69-4A strain and protein interaction was detected by cell growth in selective plates (SD-leu-trp-ura-his-ade). Scale bars: 5 μm.

Ccz1 did (Fig. 2F). In agreement with this, the exclusive vacuolar localization of Ypt7 was lost in both mutants, as observed for the GEF deletion strains (Fig. 3A) (Cabrera and Ungermann, 2013). We next asked whether the observed defect was due to complex assembly. However, neither mutation affected the formation of the dimer and we could purify Mon1–Ccz1 complexes with similar stoichiometries as observed for the wild-type complex using the established tandem-affinity purification protocol (Fig. 3B) (Nordmann et al., 2010). We then asked whether the purified mutant complexes were still functional and used the vacuole fusion assay to measure their GEF activity (Fig. 3C). In this assay, fusion of vacuoles from two different tester strains allows the protease present in one vacuole population to process immature alkaline phosphatase, which is found in the other vacuole population (Wickner, 2002). To test for GEF activity, we preincubated vacuoles with a non-specific GAP to generate Ypt7-GDP and then used Mon1–Ccz1 to reactivate Ypt7 (Nordmann et al., 2010). Whereas the wild-type Mon1–Ccz1 complex readily restored fusion, neither mutant was able to counteract GAP activity (Fig. 3C). In sum, mutations in either Mon1 or Ccz1, which had been introduced based on our homology model, maintained the GEF complex and its localization, but abolished both Ypt7 interaction and GEF activity.

The Mon1–Ccz1 complex binds negatively charged membranes

Having established that Mon1 and Ccz1 cooperate in activation of Rab7/Ypt7, we asked how activity of the complex might be regulated. Previous analyses of the *C. elegans* Mon1 protein

Journal of Cell Science (2014) 127, 1043–1051 doi:10.1242/jcs.140921

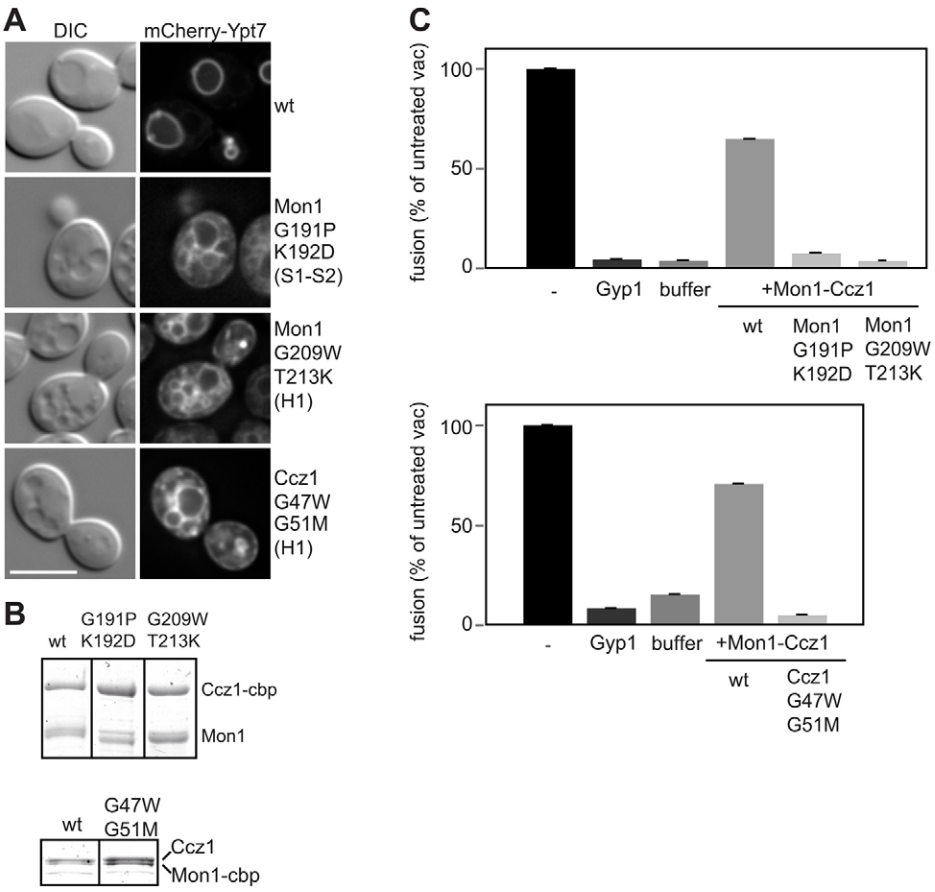

Fig. 3. Analysis of Mon1 and Ccz1 GEF mutants. (A) Localization of mCherry-tagged Ypt7 is perturbed by mutations of Mon1–Ccz1 as observed in GEF deletion strains (Cabrera and Ungermann, 2013). Ypt7 was detected by fluorescence microscopy. Scale bar: 5 μm. (B) Mon1–Ccz1 wild-type (wt) and mutant complexes were isolated using tandem-affinity purification (see Materials and Methods), resolved by SDS-PAGE, and visualized by Coomassie Blue staining. (C) Mon1 and Ccz1 mutants cannot counteract GAP activity. Vacuoles from the two tester strains were treated with the GAP Gyp1 and Mon1–Ccz1 complex where indicated. Vacuole fusion was detected after 90 minutes at 26˚C in a colorimetric enzyme assay. Values are means ± s.d.

SAND-1 indicated that it binds phosphoinositide-3-phosphate (PI3P) (Poteryaev et al., 2010), even though depletion of PI3P did not affect Mon1–Ccz1 localization in *Drosophila* (Yousefian et al., 2013). We used single Mon1 and Ccz1 proteins isolated from yeast deleted for the other binding partner, and tested their binding specificity to nitrocellulose strips coated with different lipid species (Fig. 4A). When blots were probed for Mon1 or Ccz1, we observed strong interactions with PI3P, PI5P and phosphatidylserine (PS). Interestingly, the human Mon1a protein had the same preference for PI3P and PS, indicating conserved membrane preferences of Mon1–Ccz1 across species. To confirm binding of yeast Mon1–Ccz1 to membranes with negatively charged lipids, we generated liposomes with vacuolar lipid composition with or without PI3P, incubated them with Mon1–Ccz1 complex and separated the lipid-bound fraction from the unbound by flotation (Cabrera et al., 2010). Surprisingly, Mon1–Ccz1 was mainly recovered in the liposome fraction (Fig. 4B), regardless of the presence of PI3P in the bilayer. This indicates that either Mon1–Ccz1 does not show a lipid preference or that our methodology is not sensitive enough to reveal possible differences. We thus used reflectance interference (Rif), which is a label-free detection method that determines protein binding to solid-supported membranes (Fig. 4C) (Gavutis et al., 2005). Using this experimental strategy, we observed more efficient binding of Mon1–Ccz1 to membranes containing PS and PI3P than to PC membranes (Fig. 4D, table on right). This indicates that Mon1–Ccz1 has an inherent affinity to membranes that is strengthened by negatively charged phospholipids.

Membrane association enhances Mon1–Ccz1 GEF activity to membrane-bound Ypt7

Although GEFs operate on membranes to promote both activation and localization of Rab, their activities are usually determined in solution. We wondered whether the activity of Mon1–Ccz1 might have been underestimated in our previous measurements (Nordmann et al., 2010). To mimic at least part of the Rab activation cascade, we immobilized Ypt7 tagged with C-terminal hexahistidine on vesicles containing DOGS-NTA lipids (1,2-dioleoyl-sn-glycero-3-{[N-(5-amino-1-carboxypentyl) iminodiacetic acid]succinyl}) (Sot et al., 2013), and then measured GEF activity. Unlike results obtained in solution, where modest Mon1–Ccz1 activity was observed (Nordmann et al., 2010), binding of Ypt7 to vesicles resulted in dramatically enhanced activity (Fig. 5A). We then reduced the concentration of Mon1–Ccz1, and estimated an ~1600-fold increase in GEF activity (Fig. 5B,I). Of note, the determined GEF activity of Mon1–Ccz1 without membrane-anchored Ypt7 is very similar to our previous approximation (Nordmann et al., 2010). This increase in GEF activity was dependent on the membrane localization of Ypt7 because vesicles without DOGS-NTA had no effect (Fig. 5C). As expected, the Mon1 longin mutant (G209W, T213K) and Rab5-GEF Vps9 were inactive in the GEF assay (Fig. 5D). We then asked whether the increase in membrane binding as observed before (Fig. 4D), correlated with GEF activity. We therefore generated DOGS-NTA-containing vesicles without or with PS and PI3P in different concentrations and determined GEF activity. Whereas activity was clearly observed if Ypt7 was immobilized on PC-containing membranes, it was increased twofold by the addition of negatively

Journal of Cell Science (2014) 127, 1043–1051 doi:10.1242/jcs.140921

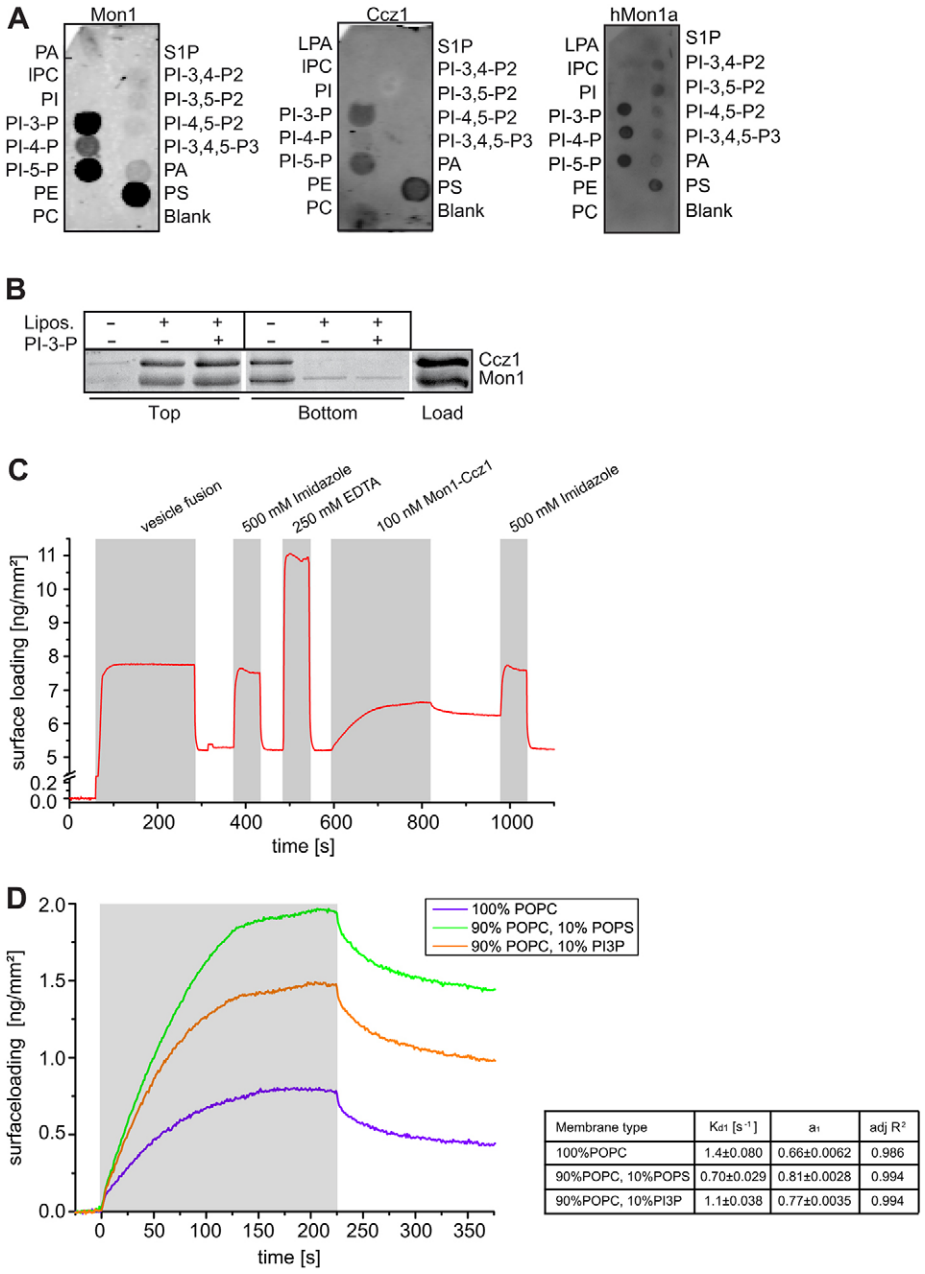

Membrane type	K_{d1} [s^{-1}]	a_1	adj R^2
100%POPC	1.4±0.080	0.66±0.0062	0.986
90%POPC, 10%POPS	0.70±0.029	0.81±0.0028	0.994
90%POPC, 10%PI3P	1.1±0.038	0.77±0.0035	0.994

Fig. 4. Mon1–Ccz1 display preference for binding to PS and PI3P lipids. (A) Mon1–Ccz1 binding to lipids. Purified yeast Mon1 and Ccz1 proteins, as well as human Mon1a, which was purified as described (Gerondopoulos et al., 2012), were incubated with lipids strips either for 1 hour at room temperature (yeast Mon1 and Ccz1) or at 4°C overnight (for hMon1a) and binding was detected by immunoblotting. Similar results were obtained with hCcz1a (not shown). (B) Mon1–Ccz1 associates with liposomes independent of the presence of PI3P. Binding of purified yeast Mon1–Ccz1 complex to liposomes with or without PI3P was monitored by flotation. (C,D) Real-time and label-free detection of Mon1–Ccz1 binding to lipid membranes. (C) Typical assay including fusion of small unilamellar lipid vesicles onto the transducer surface, conditioning of the resulting membrane, binding of purified Mon1–Ccz1 complex and elution with imidazole. The gray bars indicate the injection periods. (D) Comparison of Mon1–Ccz1 binding to membranes with different lipid compositions as indicated in C (see Materials and Methods for details). K_{d1} was calculated after normalization and fitting the dissociation phase to a double exponential. A table with the fitting values is shown to the right.

charged phospholipids (Fig. 5E,I). To discriminate whether PS and PI3P only contribute to the membrane recruitment of the GEF complex, we used a His-tagged version of the complex that can associate with membranes independently of these lipids. Interestingly, the presence of PS and PI3P resulted in additional stimulation of the GEF activity, which might reflect an additional role of these lipids in Mon1–Ccz1 activation (Fig. 5F).

The HOPS complex binds activated Ypt7 on the late endosome and vacuole, and might act in a positive-feedback loop to promote Mon1–Ccz1 activity. Indeed, the Vps39 subunit of the HOPS complex interacts with Mon1 (Wang et al., 2003; Nordmann et al., 2010), and additional interactions of metazoan Mon1 with HOPS subunits were reported (Poteryaev et al., 2010). We therefore localized GFP-tagged Mon1 or Ccz1 in cells overexpressing the entire HOPS complex. Under these conditions, Mon1 and Ccz1 accumulated on vacuolar membranes, presumably as a result of the reported interactions of the GEF complex with HOPS (Fig. 5G). We then asked if the interaction also affects activity of the GEF complex, and therefore added purified HOPS (approximately twofold excess) to the GEF assay (Fig. 5H). Even though we observed a slight increase in activity, we consider the effect rather minimal. In sum, the GEF activity of Mon1–Ccz1 is strongly increased on membranes, but is not affected by the HOPS complex.

DISCUSSION

In this study, we have addressed the molecular function of the Mon1–Ccz1 complex. Mon1–Ccz1 activity requires residues within the predicted longin domains of both subunits, which we could identify based on a homology model with the TRAPPI complex. Consistent with this, Mon1 and Ccz1 longin mutants still form a heterodimer and localize like the wild-type complex, but cannot promote nucleotide exchange in Ypt7. Using a

Journal of Cell Science (2014) 127, 1043–1051 doi:10.1242/jcs.140921

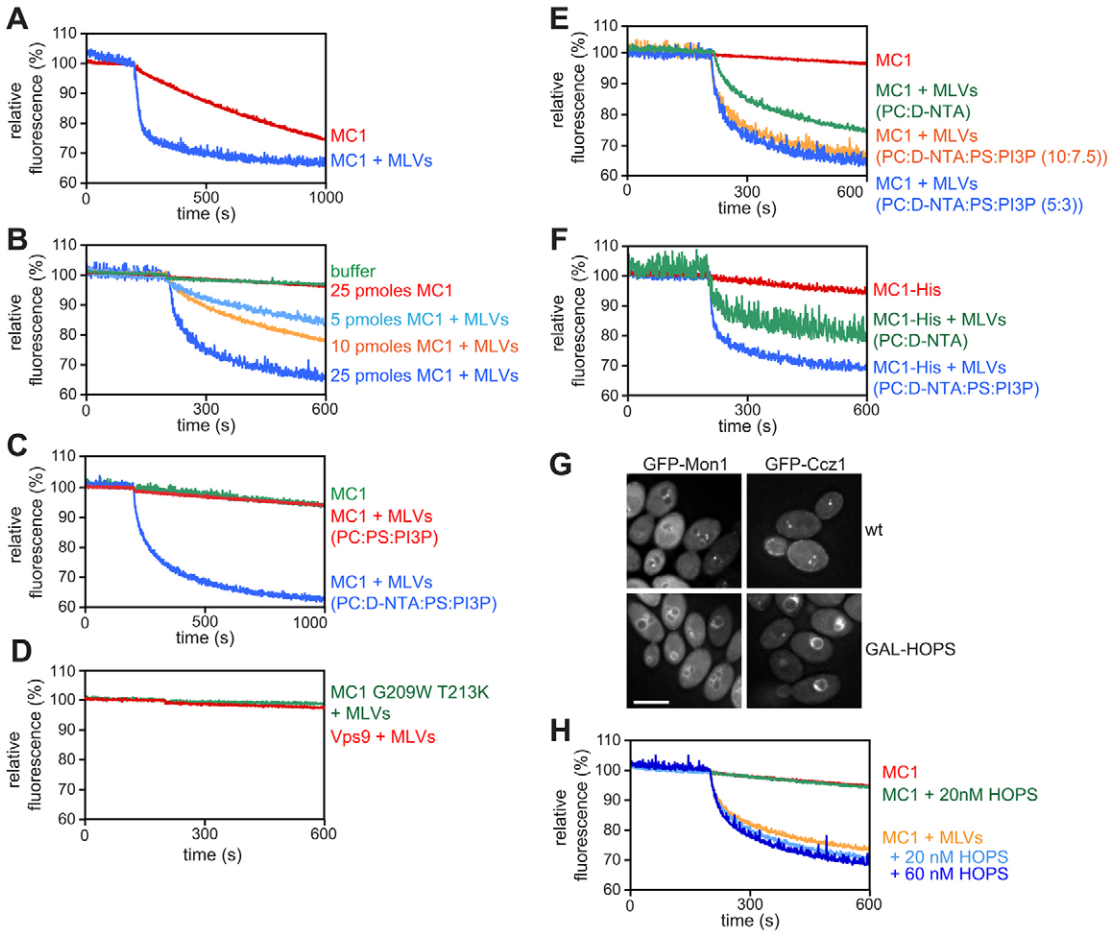

I

parameter	parameter description	MLVs with 5% PS 3% PI3P	MLVs with 10% PS 7.5% PI3P	MLVs without PS, PI3P	no MLVs
GEF [nM]	concentration in rxn.	31	31	31	625
t1 [s]	fast decay component	14	12.6	23.6	1004.8
kcat/K_M[$s^{-1}M^{-1}$]	catalytic efficiency	$2.3x10^6$	$2.56x10^6$	$1.36x10^6$	1593

Fig. 5. Mon1–Ccz1 GEF activity is stimulated by PS and PI3P lipids. 500 pmoles of Ypt7-His loaded with MANT-GDP were used in all experiments. Lipid concentration is indicated in mol% in brackets. Mon1–Ccz1 concentrations are indicated in each figure legend. (A) GEF activity of Mon1–Ccz1 towards Ypt7 is increased in the presence of POPC (52.5):DOGS-NTA(30):PS(10):PI3P(7.5) vesicles. 500 pmoles of Mon1–Ccz1 complex was used. (B) Titration of Mon1–Ccz1 complex in the GEF assay containing POPC (67.5):DOGS-NTA (15):PS(10):PI3P(7.5) vesicles. Mon1–Ccz1 complex was used at the indicated concentration. (C) Vesicles stimulate Mon1–Ccz1 GEF activity only if they contain bound Ypt7. POPC (67.5): DOGS-NTA(15):PS(10):PI3P(7.5) and POPC (82.5) PS(10):PI3P(7.5) vesicles were used in the presence of 25 pmoles of Mon1–Ccz1 complex. (D) Rab5-GEF Vps9 and Mon1 G209W, T213K-Ccz1 mutant complex are inactive towards membrane-bound Ypt7. 25 pmoles or Vps9 or Mon1 G209W T213K-Ccz1 complex were added. POPC (67.5):DOGS-NTA(15):PS(10):PI3P(7.5) vesicles were used in this assay. (E) Complete GEF stimulation requires PS and PI3P lipids. GEF activity of Mon1–Ccz1 was compared in vesicles of different composition, POPC(85):DOGS-NTA(15), POPC (67.5):DOGS-NTA(15):PS(10):PI3P(7.5) and POPC(77):DOGS-NTA(15):PS(5):PI3P(3). Mon1–Ccz1 concentration was 25 pmoles. (F) Contribution of PS and PI3P to recruitment and activation of Mon1–Ccz1. Where indicated, 25 pmoles of Mon1–Ccz1 complex carrying a His tag were added. POPC(85):DOGS-NTA(15) and POPC (67.5):DOGS-NTA(15):PS(10):PI3P(7.5) vesicles were used in the GEF assay. (G) Excess of HOPS relocalizes Mon1 and Ccz1 to the vacuole membranes. Distribution of Mon1 and Ccz1 was analyzed by fluorescence microscopy in wild-type (wt) and cells overexpressing all HOPS subunits. Scale bar: 5 μm. (H) Mon1–Ccz1 GEF activity was slightly enhanced by the HOPS complex. GEF assay included 500 pmoles of Ypt7-His loaded with MANT-GDP, 25 pmoles Mon1–Ccz1 complex, HOPS complex at the indicated concentration and POPC(85):DOGS-NTA(15) vesicles. (I) Estimation of Mon1–Ccz1 GEF activity. k_{cat}/K_m was calculated after fitting the nucleotide release curves to a double exponential curve.

modified GEF assay, we further show that Mon1–Ccz1 is strongly active once it is recruited to the membranes, suggesting that GEF activities might have been underestimated previously.

The presence of longin domains in Mon1–Ccz1 and TRAPPI, and the similar phenotype of the mutants suggest that both GEFs might share a related Rab-binding surface and nucleotide exchange mechanism. Also, the recently resolved DENND1 GEF domain contains a longin fold, although it binds Rab35 via a different surface compared with the interaction between TRAPPI and Ypt1 (Wu et al., 2011). We are aware that within the TRAPPI complex, the two Bet3 subunits contribute to the binding of Ypt1 and the C-terminal residues of Bet3A have a crucial role to

Journal of Cell Science (2014) 127, 1043–1051 doi:10.1242/jcs.140921

promote GEF activity (Cai et al., 2008). We thus consider it likely that additional segments proximal to the longin domains of Mon1–Ccz1 will be required for full activity. We also note that our model is limited by the structural differences between Ypt1 and Ypt7, especially in their N-terminal regions. However, at this point, our working model allows us to predict essential residues for GEF activity (Figs 1,2).

In this context, we realized that roadblock domains that are found in subunits of the EGO/ragulator complex have been predicted as GEFs for the Rag GTPases (BarPeled et al., 2013). Even though the order of secondary structure elements differs between roadblock and longin domains, their overall structure is quite similar (Kurzbauer et al., 2004; Qian et al., 2005; Zhang et al., 2012). These domains have probably evolved as general interactors of small GTPases (Levine et al., 2013), and a subfamily might act as dimeric GEFs. Importantly, the dimeric BLOC-3 complex also harbors a longin domain in each of its two subunits Hps1 and Hps4 and might function in a very similar manner to Mon1–Ccz1 (Gerondopoulos et al., 2012). It thus is conceivable that these domains have evolved as general interactors of small GTPases. Intriguingly, the dimeric Ric1–Rgp1 complex, which activates Ypt6 (Siniossoglou et al., 2000), also depends on both subunits for activity, and might also use a shared surface to interact with its Rab Ypt6/Rab6.

Even though we have shown GEF activity of Mon1–Ccz1 previously *in vitro*, we did not expect a 1600-fold increase in activity (k_{cat}/K_M) upon immobilization of Ypt7 on membranes. This might be due in part to the membrane recruitment of both proteins. Although the assay does not recapitulate the entire cycle, it revealed that Mon1–Ccz1 activity is far higher than previously anticipated. GEFs such as the Legionella DrrA protein have strong activity *in vitro*, which is sufficient to counteract Rab extraction by GDI (Schöbel et al., 2009; Zhu et al., 2010; Suh et al., 2010). It is thus likely that other GEFs use similar mechanisms and will explain how GEFs that are mistargeted to the mitochondria can drive the recruitment of Rabs to this organelle (Gerondopoulos et al., 2012; Blümer et al., 2013), even though some targeting information might reside in additional proteins and the Rab itself (Cabrera and Ungermann, 2013). Our adjustment in the GEF assay now provides insight into the activity of Mon1–Ccz1. We demonstrated that acidic phospholipids such as PS and PI3P clearly enhance the inherent ability of the yeast and human complex to bind membranes, in agreement with earlier findings on *C. elegans* Mon1 (Poteryaev et al., 2010). Interestingly, in *Drosophila*, the Mon1–Ccz1 complex localizes even in the absence of PI3P to membranes (Yousefian et al., 2013). We consider it likely that acidic phospholipids also facilitate the Rab-GEF interaction by optimally positioning the GEF complex relative to the Rab. We believe that similar assays with other GEFs will also uncover stronger GEF activities. A more extreme case was observed for Rasal, a RasGAP that displays activity only when it is recruited with its Ras substrate to the same membrane (Sot et al., 2013). Because GEFs function only on membranes *in vivo*, we consider our approach more suitable to mimic the *in vivo* situation on organelles.

One aspect that we could not clarify was the timing of Mon1–Ccz1 recruitment. It is possible that the complex is always active on endosomal membranes or it might be activated only once endosomes have matured, and thus can contribute to the exchange of Rab5 for Rab7 (Rink et al., 2005; Poteryaev et al., 2010). With respect to yeast, it is puzzling that the amounts of Ypt7 on endosomes are rather low, even though we observe Mon1–Ccz1 mostly on endosomes (Nordmann et al., 2010). This suggests that the complex might be further regulated *in vivo*. At this point, our data indicate that Mon1–Ccz1 acts primarily at endosomes and its interaction with HOPS might create an additional GEF microdomain on vacuoles. Within our experimental set-up, Mon1–Ccz1 activity was not strongly affected by HOPS, and Ypt7 localization was not disturbed in the absence of Vps39, which binds to Mon1 *in vitro* (Nordmann et al., 2010). We expect that the further dissection of the role of other endosomal factors that might function in a Rab cascade will help us to reveal how Mon1–Ccz1 function is controlled *in vivo*. In summary, our data reveal that the Mon1–Ccz1 GEF complex activates Ypt7 via a common interface, has highest activity on membranes and acts independently of the HOPS complex.

MATERIALS AND METHODS

Yeast strains and molecular biology

Strains and plasmids used in this study are listed in supplementary material Tables S1 and S2, respectively. Deletions and tagging of genes were done using homologous recombination of PCR fragments (Janke et al., 2004; Puig et al., 1998). mCherry-tagged Ypt7 was expressed from plasmid pRS414-TPIpr-mCherry-V5, which was generated from plasmid pRS415-TPIpr-mCherry-V5-ATG8 (a gift from Fulvio Reggiori, University Medical Center Utrecht, The Netherlands). Mon1 and Ccz1 mutants were generated using the QuikChange site-directed mutagenesis kit from Stratagene (La Jolla, CA). The catalytic domain of Gyp1 (249–637) was purified from a BL21 strain containing plasmid pET22-Gyp1-46 (Nordmann et al., 2010). Protein expression was induced by addition of 0.5 mM isopropyl-d-thiogalactoside overnight at 20°C. Purification was performed using the nickel nitrilotriacetic acid resin (Qiagen, Hilden, Germany) and elution with 300 mM imidazole.

Yeast three-hybrid assay

YEP352-Mon1, pACT2-Ccz1 and pFBT9-Ypt7 plasmids containing wild-type and mutant versions of Mon1, Ccz1 and Ypt7 were co-transformed into PJ69-4A strain and plated on minimal medium lacking leucine, tryptophan and uracil. Transformants were patched first on plates lacking leucine, tryptophan and uracil and afterwards on plates lacking leucine, tryptophan, uracil, histidine and adenine. Four clones were analyzed for each combination and one is shown.

Modeling of Mon1 and Ccz1

The Genesilico metaserver (https://genesilico.pl/meta2) (Kuroski and Bujnicki 2003) was used to identify remotely related proteins of known structure (by allowing for much more freedom in sequence alignments). Secondary structure predictions were carried out with either PredictProtein or PsiPred (http://predictprotein.org, http://bioinf.cs.ucl.ac.uk/psipred/). Both published structures of the TRAPP complex were identified (PDB IDs 3CUE 2J3T; protein data bank codes from www.pdb.org). 3CUEc and 2J3Tc (chain c of yeast and mouse Bet5 respectively) were identified for the first 150 residues of Ccz1. The server also reports Bet5 structures for the Mon1 fragment (180–287) but with a lower score. The template for modeling consisted of Ypt7-GDP (PDB ID 1KY3) (Constantinescu et al., 2002) and mammalian Bet5 and Trs23 (PDB ID 2J3T) and was obtained by 3D alignment with the respective chains of Ypt1/TRAPP structure (PDB ID 3CUE). A PDZL domain, which is absent in yeast Trs23 was removed from the template. The complex formed by Ypt7 GDP and the longin domains of Mon1 and Ccz1 was modeled using YASARA 13.4.21 (Krieger et al., 2002). The resulting model resembled the Ypt1–Trs23–Bet5 structure and showed only few clashes in the contacting residues. The model scored as optimal or satisfactory considering the correctness of backbone (Ramachandran plot) and side-chain dihedrals, as well as packing interactions. Note that the model does not include Ypt7 residues (38–40 and 67–76), which are missing in the reported structure.

Microscopy

Yeast cells were grown to mid-log phase in YPD, YPG or synthetic complete (SDC) medium lacking selected amino acids or nucleotides, collected by centrifugation, washed once with SDC or SGC medium supplemented with all amino acids, and immediately analyzed by fluorescence microscopy. For FM4-64 staining of vacuoles, cells were incubated with 30 µM FM4-64 for 30 minutes, washed twice with YPD medium, and incubated in the same medium without dye for 1 hour. Images were acquired with a Leica DM5500 B microscope equipped with a SPOT Pursuit camera equipped with an internal filter wheel (D460sp, BP460-515 and D580lp; Leica Microsystems GmbH), fluorescence filters [49002 ET-GFP (FITC/Cy2): Exc. ET470/40x, Em. ET525/50m; Wide Green: Exc. D535/50, Em. E590lp; 49008 ET-mCherry, Texas Red: Exc. ET560/40x, Em. ET630/75m Chroma Technology Corp.], and Metamorph 7 software (Visitron Systems, Munich, Germany). Images were processed using ImageJ 1.42 (National Institutes of Health) and Autoquant x v1.3.3 (Media Cybernetics, Inc.).

Tandem affinity purification (TAP)

Tandem affinity purification was performed as described (Nordmann et al., 2010; Ostrowicz et al., 2010; Bröcker et al., 2012). Three liters of culture were grown at 30℃ to OD_{600} ~4 and cells were harvested by centrifugation. Cells were lysed in buffer containing 50 mM HEPES-NaOH, pH 7.4, 300 mM NaCl, 1.5 mM $MgCl_2$, 1× FY protease inhibitor mix (Serva, Heidelberg, Germany), 0.5 mM PMSF and 1 mM DTT. Lysates were centrifuged for 90 minutes at 100,000 ***g***, and supernatants were incubated with IgG Sepharose beads for 2 hours at 4℃. Beads were isolated by centrifugation at 800 ***g*** for 5 minutes, and washed with 15 ml lysis buffer containing 0.5 mM DTT. Bound proteins were eluted by TEV cleavage, and analyzed on SDS-PAGE. For Mon1–Ccz1, buffer exchange via NAP5 columns to the fusion reaction buffer was performed. For HOPS, buffer exchange was omitted.

Vacuole fusion

Vacuoles were isolated from yeast strains BJ3505 (*pep4Δ*) and DKY6281 (*pho8Δ*) via ficoll gradient centrifugation as described (Cabrera and Ungermann 2008). Fusion reactions containing 3 µg of each vacuole type were incubated in fusion reaction buffer (1 mM PIPES-KOH, pH 6.8, 20 mM sorbitol, 5 mM $MgCl_2$, 125 mM KCl), 10 µM CoA, 0.01 µg His-Sec18, 1 mM GTP, with or without ATP-regenerating system (0.5 mM ATP, 40 mM creatine phosphate, 0.1 mg/ml creatine kinase) for 90 minutes at 27℃ and developed for 5 minutes. Where indicated, Mon1–Ccz1 or recombinant Gyp1-46 was added. Fusion values correspond to the average of 2–4 samples.

Interaction of Mon1–Ccz1 with lipids

Single Mon1 and Ccz1 molecules were purified from strains lacking the respective binding partner. Proteins were incubated with the lipid strips (Invitrogen) that had been blocked with TBS-Tween and 3% fatty acid free BSA for 1 hour at room temperature and protein binding detected by immunoblotting. Purification of human Mon1a was done as described (Gerondopoulos et al., 2012). Blots were blocked with TBS-Tween and 3% fatty acid free BSA as described by the manufacturer (Invitrogen). Incubation with human Mon1–Ccz1 was carried out at 4℃ overnight.

Vesicle isolation

Lipids were purchased from Avanti Polar Lipids, except ergosterol (Sigma) and phosphatidylinositol-3-phosphate (PI3P) (Mobitech/Echelon). A vacuolar lipid mixture (Zinser et al., 1991; Mima et al., 2008) containing (mol %) di-oleoyl-phosphatidylcholine (DOPC; 47%), di-oleoyl-phosphatidyl-ethanolamine (DOPE; 18%), soy phosphatidyl-inositol (PI; 18%), di-oleoyl-phosphatidyl-serine (DOPS; 4.4%), di-oleoyl-phosphatidic acid (DOPA; 2%), cardiolipin (1.6%), ergosterol (8%), diacylglycerol (DAG; 1%) and NBD-PE (1%) was prepared by evaporation, and resuspended in HEPES-KOAc (HK) buffer (50 mM HEPES-KOH, pH 7.2 and 120 mM KOAc). Where indicated, phosphatidylinositol-3-phosphate (PI3P, 1%) was added. After five steps of thawing and freezing in liquid nitrogen, the liposome suspension (2 mM) was extruded through polycarbonate filters of 400, 200, 100 nm pore size using a hand extruder (Avanti). The liposome size was determined by dynamic light scattering (DynaPro Titan, Wyatt Technology Europe GmbH, Dernbach, Germany). To obtain the vesicles used in the GEF assays, the lipid mixture was prepared by evaporation of the desired lipids, resuspended in HEPES-NaCl buffer containing 20 mM HEPES-NaOH, pH 7.4, 150 mM NaCl, and 1 mM $MgCl_2$ to a final concentration of 3 mM, and subjected to nine steps of thawing and freezing in liquid nitrogen.

Liposome flotation assay

The assay was performed as described (Cabrera et al., 2010). In brief, purified Mon1–Ccz1 complex (200 nM) was incubated with liposomes (0.75 mM) in 150 µl HKM buffer (HK buffer with 1 mM $MgCl_2$) at room temperature for 5 minutes. 100 µl of a 75% sucrose solution in HKM buffer was added to adjust the sucrose concentration to 30%. The suspension was overlaid with two layers (200 µl of 25% sucrose solution in HKM and 50 µl HKM buffer). Gradients were centrifuged at 220,000 ***g*** for 1 hour at 20℃. Proteins from the bottom (250 µl) and top (50 µl) fractions were trichloroacetic acid (TCA)-precipitated, analyzed by SDS-PAGE and Sypro Orange staining (Invitrogen). Protein binding was detected using VersaDoc imaging system (Bio-Rad GmbH, Munich).

Real-time membrane-binding studies

Binding of Mon1–Ccz1 to artificial membranes was monitored in real time by reflectance interference (RIf) detection in a flow system as in principle described previously (Gavutis et al., 2005). Briefly, RIf allows label-free detection of protein binding to the surface of a glass substrate coated with a thin silica layer. All experiments were carried with HEPES-NaCl buffer (20 mM HEPES, pH 7.5, 150 mM NaCl) as running buffer. Continuous membranes were obtained by fusing small unilamellar lipid vesicles composed of POPC only, 90% POPC and 10% POPS or 90% POPC and 10% PI3P, onto clean transducer slides. Prior to each measurement the system and membrane were washed by successive injections of imidazole (500 mM, 250 µl, 86 seconds) and EDTA (250 mM, 250 µl, 86 seconds). Subsequently, 100 nM of the Mon1–Ccz1 complex was injected in a volume of 250 µl for 185 seconds, and its dissociation was monitored for 150 seconds by rinsing with HBS. A final washing step with imidazole removed all the bound protein from the membrane to recover it for the next measurement and served as proof of an intact bilayer.

GEF assay on vesicles

GEF assays were performed as described (Nordmann et al., 2010). Briefly, 500 pmoles of the Rab Ypt7-His were preloaded with MANT-GDP, and incubated with 160 µl vesicles for 10 minutes at 25℃ before incubation with different amounts of Mon1–Ccz1 complex. MANT fluorescence was recorded for the indicated time in a fluorimeter with a temperature-controlled cuvette and a stirring device (Jasco, Gross-Umstadt, Germany). Samples were excited at 366 nm and fluorescence was detected at 443 nm. After 200 seconds, GTP was added to final concentrations of 0.1 mM to trigger the exchange reaction. The decrease of MANT-GDP fluorescence is used as read-out of nucleotide release.

Acknowledgements

We would like to thank Daniel Kümmel for feedback on the manuscript, and all members of the Ungermann lab for critical suggestions.

Competing interests

The authors declare no competing financial interests.

Author contributions

M.C., M.N, F.B, S.E.V. and C.U. designed research; M.C., M.N., A.P., D.S., A.G. and S.E.V. performed research; M.C., M.N., D.S., A.G., F.B., J.P., S.E.V. and C.U. analyzed data; M.C., S.E.V. and C.U. wrote the paper.

Funding

This work was supported by the SFB (Sonderforschungsbereich) 944 (project P11); and the Hans-Mühlenhoff foundation (to C.U.). J.P. is funded by the SFB

944 (project P9); F.B. received support from the Wellcome Trust [grant number 082467/Z/07/Z]. Deposited in PMC for release after 6 months.

Supplementary material

Supplementary material available online at
http://jcs.biologists.org/lookup/suppl/doi:10.1242/jcs.140921/-/DC1

References

Allaire, P. D., Marat, A. L., Dall'Armi, C., Di Paolo, G., McPherson, P. S. and Ritter, B. (2010). The Connecdenn DENN domain: a GEF for Rab35 mediating cargo-specific exit from early endosomes. *Mol. Cell* **37**, 370-382.

Bar-Peled, L., Chantranupong, L., Cherniack, A. D., Chen, W. W., Ottina, K. A., Grabiner, B. C., Spear, E. D., Carter, S. L., Meyerson, M. and Sabatini, D. M. (2013). A Tumor suppressor complex with GAP activity for the Rag GTPases that signal amino acid sufficiency to mTORC1. *Science* **340**, 1100-1106.

Barr, F. A. (2013). Review series: Rab GTPases and membrane identity: causal or inconsequential? *J. Cell Biol.* **202**, 191-199.

Blümer, J., Rey, J., Dehmelt, L., Mazel, T., Wu, Y. W., Bastiaens, P., Goody, R. S. and Itzen, A. (2013). RabGEFs are a major determinant for specific Rab membrane targeting. *J. Cell Biol.* **200**, 287-300.

Boriack-Sjodin, P. A., Margarit, S. M., Bar-Sagi, D. and Kuriyan, J. (1998). The structural basis of the activation of Ras by Sos. *Nature* **394**, 337-343.

Bröcker, C., Kuhlee, A., Gatsogiannis, C., Balderhaar, H. J., Hönscher, C., Engelbrecht-Vandré, S., Ungermann, C. and Raunser, S. (2012). Molecular architecture of the multisubunit homotypic fusion and vacuole protein sorting (HOPS) tethering complex. *Proc. Natl. Acad. Sci. USA* **109**, 1991-1996.

Cabrera, M. and Ungermann, C. (2008). Purification and in vitro analysis of yeast vacuoles. *Methods Enzymol.* **451**, 177-196.

Cabrera, M. and Ungermann, C. (2013). Guanine nucleotide exchange factors (GEFs) have a critical but not exclusive role in organelle localization of Rab GTPases. *J. Biol. Chem.* **288**, 28704-28712.

Cabrera, M., Langemeyer, L., Mari, M., Rethmeier, R., Orban, I., Perz, A., Bröcker, C., Griffith, J., Klose, D., Steinhoff, H.-J. et al. (2010). Phosphorylation of a membrane curvature-sensing motif switches function of the HOPS subunit Vps41 in membrane tethering. *J. Cell Biol.* **191**, 845-859.

Cai, Y., Chin, H. F., Lazarova, D., Menon, S., Fu, C., Cai, H., Sclafani, A., Rodgers, D. W., De La Cruz, E. M., Ferro-Novick, S. et al. (2008). The structural basis for activation of the Rab Ypt1p by the TRAPP membrane-tethering complexes. *Cell* **133**, 1202-1213.

Constantinescu, A. T., Rak, A., Alexandrov, K., Esters, H., Goody, R. S. and Scheidig, A. J. (2002). Rab-subfamily-specific regions of Ypt7p are structurally different from other RabGTPases. *Structure (Camb)* **10**, 569-579.

Delprato, A. and Lambright, D. G. (2007). Structural basis for Rab GTPase activation by VPS9 domain exchange factors. *Nat. Struct. Mol. Biol.* **14**, 406-412.

Delprato, A., Merithew, E. and Lambright, D. G. (2004). Structure, exchange determinants, and family-wide rab specificity of the tandem helical bundle and Vps9 domains of Rabex-5. *Cell* **118**, 607-617.

Dong, G., Medkova, M., Novick, P. and Reinisch, K. M. (2007). A catalytic coiled coil: structural insights into the activation of the Rab GTPase Sec4p by Sec2p. *Mol. Cell* **25**, 455-462.

Gavutis, M., Lata, S., Lamken, P., Müller, P. and Piehler, J. (2005). Lateral ligand-receptor interactions on membranes probed by simultaneous fluorescence-interference detection. *Biophys. J.* **88**, 4289-4302.

Gerondopoulos, A., Langemeyer, L., Liang, J.-R., Linford, A. and Barr, F. A. (2012). BLOC-3 mutated in Hermansky-Pudlak syndrome is a Rab32/38 guanine nucleotide exchange factor. *Curr. Biol.* **22**, 2135-2139.

Hutagalung, A. H. and Novick, P. J. (2011). Role of Rab GTPases in membrane traffic and cell physiology. *Physiol. Rev.* **91**, 119-149.

Itzen, A. and Goody, R. S. (2011). GTPases involved in vesicular trafficking: structures and mechanisms. *Semin. Cell Dev. Biol.* **22**, 48-56.

Janke, C., Magiera, M. M., Rathfelder, N., Taxis, C., Reber, S., Maekawa, H., Moreno-Borchart, A., Doenges, G., Schwob, E., Schiebel, E. et al. (2004). A versatile toolbox for PCR-based tagging of yeast genes: new fluorescent proteins, more markers and promoter substitution cassettes. *Yeast* **21**, 947-962.

Kim, Y. G., Raunser, S., Munger, C., Wagner, J., Song, Y. L., Cygler, M., Walz, T., Oh, B. H. and Sacher, M. (2006). The architecture of the multisubunit TRAPP I complex suggests a model for vesicle tethering. *Cell* **127**, 817-830.

Kinchen, J. M. and Ravichandran, K. S. (2010). Identification of two evolutionarily conserved genes regulating processing of engulfed apoptotic cells. *Nature* **464**, 778-782.

Krieger, E., Koraimann, G. and Vriend, G. (2002). Increasing the precision of comparative models with YASARA NOVA – a self-parameterizing force field. *Proteins* **47**, 393-402.

Kümmel, D., Muller, J., Roske, Y., Henke, N. and Heinemann, U. (2006). Structure of the Bet3-Tpc6B core of TRAPP: two Tpc6 paralogs form trimeric complexes with Bet3 and Mum2. *J. Mol. Biol.* **361**, 22-32.

Kurowski, M. A. and Bujnicki, J. M. (2003). GeneSilico protein structure prediction meta-server. *Nucleic Acids Res.* **31**, 3305-3307.

Kurzbauer, R., Teis, D., de Araujo, M. E., Maurer-Stroh, S., Eisenhaber, F., Bourenkov, G. P., Bartunik, H. D., Hekman, M., Rapp, U. R., Huber, L. A. et al. (2004). Crystal structure of the p14/MP1 scaffolding complex: how a twin couple attaches mitogen-activated protein kinase signaling to late endosomes. *Proc. Natl. Acad. Sci. USA* **101**, 10984-10989.

Lachmann, J., Ungermann, C. and Engelbrecht-Vandré, S. (2011). Rab GTPases and tethering in the yeast endocytic pathway. *Small GTPases* **2**, 182-186.

Levine, T. P., Daniels, R. D., Wong, L. H., Gatta, A. T., Gerondopoulos, A. and Barr, F. A. (2013). Discovery of new Longin and Roadblock domains that form platforms for small GTPases in Ragulator and TRAPP-II. *Small GTPases* **4**, 62-69.

Marat, A. L., Dokainish, H. and McPherson, P. S. (2011). DENN domain proteins: regulators of Rab GTPases. *J. Biol. Chem.* **286**, 13791-13800.

Mima, J., Hickey, C. M., Xu, H., Jun, Y. and Wickner, W. (2008). Reconstituted membrane fusion requires regulatory lipids, SNAREs and synergistic SNARE chaperones. *EMBO J.* **27**, 2031-2042.

Nordmann, M., Cabrera, M., Perz, A., Bröcker, C., Ostrowicz, C., Engelbrecht-Vandré, S. and Ungermann, C. (2010). The Mon1-Ccz1 complex is the GEF of the late endosomal Rab7 homolog Ypt7. *Curr. Biol.* **20**, 1654-1659.

Ostrowicz, C. W., Bröcker, C., Ahnert, F., Nordmann, M., Lachmann, J., Peplowska, K., Perz, A., Auffarth, K., Engelbrecht-Vandré, S. and Ungermann, C. (2010). Defined subunit arrangement and rab interactions are required for functionality of the HOPS tethering complex. *Traffic* **11**, 1334-1346.

Poteryaev, D., Datta, S., Ackema, K., Zerial, M. and Spang, A. (2010). Identification of the switch in early-to-late endosome transition. *Cell* **141**, 497-508.

Puig, O., Rutz, B., Luukkonen, B. G., Kandels-Lewis, S., Bragado-Nilsson, E. and Séraphin, B. (1998). New constructs and strategies for efficient PCR-based gene manipulations in yeast. *Yeast* **14**, 1139-1146.

Pusapati, G. V., Luchetti, G. and Pfeffer, S. R. (2012). Ric1-Rgp1 complex is a guanine nucleotide exchange factor for the late Golgi Rab6A GTPase and an effector of the medial Golgi Rab33B GTPase. *J. Biol. Chem.* **287**, 42129-42137.

Qian, C., Zhang, Q., Wang, X., Zeng, L., Farooq, A. and Zhou, M. M. (2005). Structure of the adaptor protein p14 reveals a profilin-like fold with distinct function. *J. Mol. Biol.* **347**, 309-321.

Rink, J., Ghigo, E., Kalaidzidis, Y. and Zerial, M. (2005). Rab conversion as a mechanism of progression from early to late endosomes. *Cell* **122**, 735-749.

Sato, Y., Fukai, S., Ishitani, R. and Nureki, O. (2007). Crystal structure of the Sec4p.Sec2p complex in the nucleotide exchanging intermediate state. *Proc. Natl. Acad. Sci. USA* **104**, 8305-8310.

Schöbel, S., Oesterlin, L. K., Blankenfeldt, W., Goody, R. S. and Itzen, A. (2009). RabGDI displacement by DrrA from Legionella is a consequence of its guanine nucleotide exchange activity. *Mol. Cell* **36**, 1060-1072.

Siniossoglou, S., Peak-Chew, S. Y. and Pelham, H. R. (2000). Ric1p and Rgp1p form a complex that catalyses nucleotide exchange on Ypt6p. *EMBO J.* **19**, 4885-4894.

Sot, B., Behrmann, E., Raunser, S. and Wittinghofer, A. (2013). Ras GTPase activating (RasGAP) activity of the dual specificity GAP protein Rasal requires colocalization and C2 domain binding to lipid membranes. *Proc. Natl. Acad. Sci. USA* **110**, 111-116.

Suh, H.-Y., Lee, D.-W., Lee, K.-H., Ku, B., Choi, S.-J., Woo, J.-S., Kim, Y.-G. and Oh, B.-H. (2010). Structural insights into the dual nucleotide exchange and GDI displacement activity of SidM/DrrA. *EMBO J.* **29**, 496-504.

Wang, C.-W., Stromhaug, P. E., Shima, J. and Klionsky, D. J. (2002). The Ccz1-Mon1 protein complex is required for the late step of multiple vacuole delivery pathways. *J. Biol. Chem.* **277**, 47917-47927.

Wang, C.-W., Stromhaug, P. E., Kauffman, E. J., Weisman, L. S. and Klionsky, D. J. (2003). Yeast homotypic vacuole fusion requires the Ccz1-Mon1 complex during the tethering/docking stage. *J. Cell Biol.* **163**, 973-985.

Wickner, W. (2002). Yeast vacuoles and membrane fusion pathways. *EMBO J.* **21**, 1241-1247.

Wu, X., Bradley, M. J., Cai, Y. and Kümmel, D., De La Cruz, E. M., Barr, F. A. and Reinisch, K. M. (2011). Insights regarding guanine nucleotide exchange from the structure of a DENN-domain protein complexed with its Rab GTPase substrate. *Proc. Natl. Acad. Sci. USA* **108**, 18672-18677.

Yoshimura, S., Gerondopoulos, A., Linford, A., Rigden, D. J. and Barr, F. A. (2010). Family-wide characterization of the DENN domain Rab GDP-GTP exchange factors. *J. Cell Biol.* **191**, 367-381.

Yousefian, J., Troost, T., Grawe, F., Sasamura, T., Fortini, M. and Klein, T. (2013). Dmon1 controls recruitment of Rab7 to maturing endosomes in Drosophila. *J. Cell Sci.* **126**, 1583-1594.

Zhang, T., Péli-Gulli, M.-P., Yang, H., De Virgilio, C. and Ding, J. (2012). Ego3 functions as a homodimer to mediate the interaction between Gtr1-Gtr2 and Ego1 in the ego complex to activate TORC1. *Structure* **20**, 2151-2160.

Zhu, Y., Hu, L., Zhou, Y., Yao, Q., Liu, L. and Shao, F. (2010). Structural mechanism of host Rab1 activation by the bifunctional Legionella type IV effector SidM/DrrA. *Proc. Natl. Acad. Sci. USA* **107**, 4699-4704.

Zinser, E., Sperka-Gottlieb, C. D., Fasch, E. V., Kohlwein, S. D. and Paltauf Fand Daum, G. (1991). Phospholipid synthesis and lipid composition of subcellular membranes in the unicellular eukaryote Saccharomyces cerevisiae. *J. Bacteriol.* **173**, 2026-2034.

Supplemental material (Cabrera et al.)

Table S1 – Strains used in this study

Strain	Genotype	Reference
CUY1	BJ3505 MATa *pep4Δ::HIS3 prb1-Δ1.6R lys2-208 trp1*Δ101 *ura3-52 gal2*	Haas et al., 1995
CUY764	BY4741 *MATa his3*Δ1 *leu2*Δ0 *met15*Δ0 *ura3*Δ0	EUROSCARF library
CUY105	BY4732 *MATa his3*Δ200 *leu2*Δ0 *met15*Δ0 *trp1*Δ63 *ura3*Δ0	EUROSCARF library
CUY94	BY4720 *MATα lys2*Δ0 *trp1*Δ63 *ura3*Δ0	EUROSCARF library
CUY2694	BY4727 *MATalpha his3Δ200 leu2Δ0 lys2Δ0 met15Δ0 trp1Δ63 ura3Δ0*	EUROSCARF library
CUY1620	PJ69-4A	Haas et al., 2005
CUY2470	BY4732 *GAL1pr-CCZ1-TAP GAL1pr-MON1*	Nordmann et al., 2010
CUY4097	*BY4732 GAL1pr-CCZ1 GAL1pr-MON1-TAP*	Nordmann et al., 2010
CUY3623	BY4741 *GAL1pr-CCZ1-TAP mon1*Δ	Nordmann et al., 2010
CUY3624	BY4732 *GAL1pr-MON1-TAP ccz1*Δ	Nordmann et al., 2010
CUY6301	BY4741 *mon1*Δ *GAL1pr-CCZ1-TAP pRS406-GAL1pr-MON1 G191P*	This study
CUY6589	BY4741 *mon1*Δ *GAL1pr-CCZ1-TAP pRS406-GAL1pr-MON1 K192D*	This study
CUY6302	BY4741 *mon1*Δ *GAL1pr-CCZ1-TAP pRS406-GAL1pr-*MON1 *G191P K192D*	This study
CUY7782	BJ3505 *pRS406-NOP1pr-GFP-MON1 G191P K192D*	This study
CUY6880	BJ3505 *mon1Δ pRS406-NOP1pr-MON1 G191P K192D*	This study
CUY6588	BY4741 *mon1*Δ *GAL1pr-CCZ1-TAP pRS406-GAL1pr-MON1 G209W*	This study
CUY7117	BY4741 *mon1*Δ *GAL1pr-CCZ1-TAP pRS406-GAL1pr-MON1 G209W T213K*	This study
CUY7786	BJ3505 *pRS406-NOP1pr-GFP-MON1 G209W T213K*	This study
CUY7791	BJ3505 *mon1Δ pRS406-NOP1pr-MON1 G209W T213K*	This study
CUY7355	BY4732 *GAL1pr-MON1 ccz1*Δ *pRS406-GAL1pr-CCZ1 S12K S14K*	This study
CUY6592	BY4732 *ccz1*Δ *GAL1pr-MON1-TAP pRS406-GAL1pr-CCZ1 G47W*	This study
CUY6593	BY4732 *ccz1*Δ *GAL1pr-MON1-TAP pRS406-GAL1pr-CCZ1 G51M*	This study
CUY7582	BY4732 *ccz1*Δ *GAL1pr-MON1-TAP pRS406-GAL1pr-CCZ1 G47W G51M*	This study
CUY7788	BJ3505 *pRS406-NOP1pr-GFP-CCZ1 G47W G51M*	This study
CUY7818	BJ3505 *ccz1*Δ *pRS406-NOP1pr-CCZ1 G47W G51M*	This study
CUY8348	BY4720/BY4732 *PHO5pr-GFP-MON1*	This study
CUY8350	BY4727/BY4732 *GAL1pr-VPS41 GAL1pr-VPS39 GAL1pr-VPS33 GAL1pr-VPS11 GAL1pr-VPS16 GAL1pr-3HA-VPS18 PHO5pr-GFP-MON1*	This study
CUY8349	BY4720/BY4732 *PHO5pr-GFP-CCZ1*	This study
CUY8351	BY4727/BY4732 *GAL1pr-VPS41 GAL1pr-VPS39 GAL1pr-VPS33 GAL1pr-VPS11 GAL1pr-VPS16 GAL1pr-3HA-VPS18 PHO5pr-GFP-CCZ1*	This study

Table S2 – Plasmids used in this study

Number	Plasmid Name	Reference
1477	*pFBT9-ADH1pr-YPT7*	Markgraf et al., 2009
2049	*pACT2-ADH1pr -CCZ1*	Nordmann et al., 2010
3575	*pACT2-ADH1pr -CCZ1 G47W G51M*	This study
2910	*YEP352-ADH1pr-NLS-MON1*	This study
3744	*YEP352-ADH1pr-NLS-MON1 G191P K192D*	This study
3745	*YEP352-ADH1pr-NLS-MON1 G209W T213K*	This study
2796	*pRS414-TPIpr-mCherry-V5-YPT7*	This study
3156	*pRS406-GAL1pr-MON1 G191P*	This study
3275	*pRS406-GAL1pr-MON1 K192D*	This study
3166	*pRS406-GAL1pr-*MON1 *G191P K192D*	This study
3304	*pRS406-NOP1pr-MON1 G191P K192D*	This study
3483	*pRS406-NOP1pr-GFP-MON1 G191P K192D*	This study
3274	*pRS406-GAL1pr-MON1 G209W*	This study
3337	*pRS406-GAL1pr-MON1 G209W T213K*	This study
3479	*pRS406-NOP1pr-MON1 G209W T213K*	This study
3487	*pRS406-NOP1pr-GFP-MON1 G209W T213K*	This study
3345	*pRS406-GAL1pr-CCZ1 S12K S14K*	This study
3265	*pRS406-GAL1pr-CCZ1 G47W*	This study
3266	*pRS406-GAL1pr-CCZ1 G51M*	This study
3336	*pRS406-GAL1pr-CCZ1 G47W G51M*	This study
3478	*pRS406-NOP1pr-CCZ1 G47W G51M*	This study
3495	*pRS406-NOP1pr-GFP-CCZ1 G47W G51M*	This study